


GlassNet: Label Decoupling-based Three-stream Neural Network for Robust Image Glass Detection

Chengyu Zheng¹ , Ding Shi¹, Xuefeng Yan¹, Dong Liang¹, Mingqiang Wei^{1†}, Xin Yang², Yanwen Guo³ and Haoran Xie⁴

¹Nanjing University of Aeronautics and Astronautics, Nanjing, China

²Dalian University of Technology, Dalian, China

³Nanjing University, Nanjing, China

⁴Lingnan University, Hong Kong SAR, China

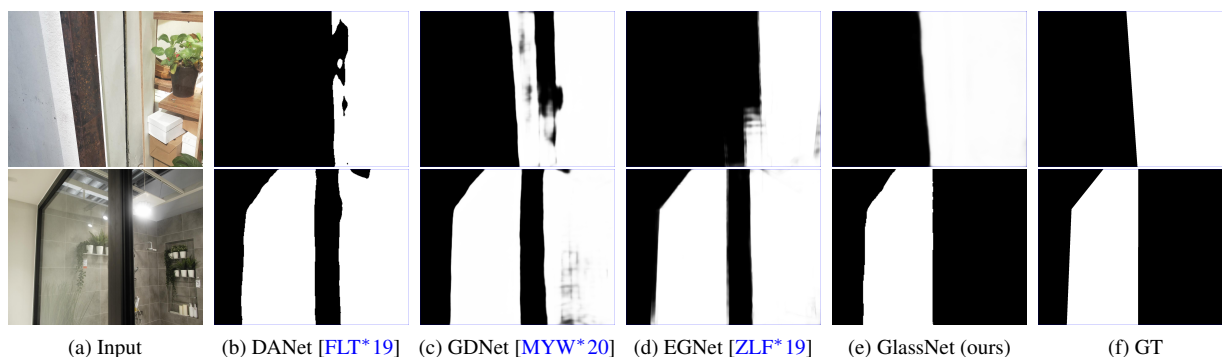


Figure 1: GlassNet compares with its competitors on the public GDD dataset [MYW*20]. Current vision systems do not sense the presence of glass effectively, since a glass region has no fixed patterns (e.g., various objects will appear behind the glass, resulting in the same appearance of the glass and the objects behind the glass in an image). DANet commonly fails to detect the glass; GDNet leads to inaccurate glass boundaries; EGNet yields wrong detection regions; while the proposed GlassNet operates smoothly on these two challenging images, where the glass is exactly detected and its boundaries are clearer. Please note that the white region corresponds to the detected glass, and the black region means the detected background.

Abstract

Most of the existing object detection methods generate poor glass detection results, due to the fact that the transparent glass shares the same appearance with arbitrary objects behind it in an image. Different from traditional deep learning-based wisdoms that simply use the object boundary as auxiliary supervision, we exploit label decoupling to decompose the original labeled ground-truth (GT) map into an interior-diffusion map and a boundary-diffusion map. The GT map in collaboration with the two newly generated maps breaks the imbalanced distribution of the object boundary, leading to improved glass detection quality. We have three key contributions to solve the transparent glass detection problem: (1) We propose a three-stream neural network (call GlassNet for short) to fully absorb beneficial features in the three maps. (2) We design a multi-scale interactive dilation module to explore a wider range of contextual information. (3) We develop an attention-based boundary-aware feature Mosaic module to integrate multi-modal information. Extensive experiments on the benchmark dataset exhibit clear improvements of our method over SOTAs, in terms of both the overall glass detection accuracy and boundary clearness.

CCS Concepts

• Computing methodologies → Object detection;

1. Introduction

Transparent glass is widely used in our daily life, such as glass windows/doors and many other glass products. However, it commonly

[†] M. Wei is the corresponding author.

hinders many vision-related tasks like depth prediction, instance segmentation, refraction removal, and object detection, etc. For example, when an intelligent robot or an unmanned plane operates automatically, they should avoid crashing into the glass to cause damages. It is, therefore, essential to accurately detect the overall glass with its boundary clearly from single images. Unfortunately, most of the existing object detection methods generate inaccurate or even wrong regions of the glass with fuzzy boundaries, due to the fact that the glass is transparent. That means, a glass region nearly has no fixed patterns; the pattern is determined by the arbitrarily appeared object behind the glass. Therefore, unlike many other objects which have relatively fixed patterns to detect more easily, the same appearance between the glass region and the objects behind it makes existing object detection methods work ineffectively. We list three representative detection approaches in Figure 1, i.e., DANet [FLT*19] for semantic segmentation, EGNet [ZLF*19] for edge-guided salient object detection, GDNet [MYW*20] for glass detection, as well as our proposed GlassNet. As shown, DANet wrongly considers the background as the glass; EGNet also yields wrong detection regions; although GDNet [MYW*20] pioneers to automatically detect glass from single images, it leads to inaccurate glass boundaries; while the proposed network operates smoothly on these two challenging images: the glass is exactly detected with its clearer boundaries by GlassNet.

Intuitively, like other vision tasks, a straightforward solution to enhance the glass detection ability, is to use boundaries of the glass as auxiliary supervision. However, in an image with glass in it, the glass-boundary pixels are much rarer than other pixels. Such a very unbalanced distribution of the glass-boundary pixels will introduce large prediction errors around the glass boundary. To this end, we arise an intriguing question that if the glass boundary diffuses itself into the glass's interior and the interior diffuses itself from its center to boundary, a deep network can better focus on regions around the glass boundary and concentrate on center areas of the glass object? To answer it, 1) we first use label decoupling (LD) [WWW*20] to explicitly decompose the original glass map into an interior-diffusion map and a boundary-diffusion map, where the first map is concentrated in the center of glass objects and the second map focuses on regions around glass boundaries; 2) based on the three different types of label information, we propose a three-stream neural network for robust glass detection (GlassNet). For the interior-diffusion stream, we only use the highest two-level image features with rich semantic information to locate the glass region; for the boundary-diffusion stream, all levels of information are aggregated to make the detection result more accurate; for the original glass stream, we utilize the lowest two-level image features with more detailed information and highest-level image features to predict the final glass maps.

Meanwhile, we design a multi-scale interactive dilation module with a large receiving field to integrate the features from adjacent levels. And we propose an attention-based boundary fuse module to merge the boundary and glass features. We have tested all the approaches on the benchmark dataset GDD [MYW*20] and our GlassNet achieves a very competitive performance. In summary, our contributions are mainly four-fold:

- We observe that in an image with glass in it, the glass-boundary

pixels are much rarer than other pixels. Such a very imbalanced distribution of the glass-boundary pixels introduces large prediction errors around the glass boundary when performing object detection. To break such an imbalanced distribution between glass-boundary pixels and non-glass-boundary pixels, we utilize the label decoupling procedure to decompose a glass label into an interior-diffusion map and a boundary-diffusion map to supervise the network training.

- We propose a three-stream network, called GlassNet, which is enhanced by label decoupling features to produce more precise glass maps.
- We design a multi-scale interactive dilation module to explore a wider range of contextual information and a attention-based boundary-aware feature Mosaic module to integrate multi-modal information.
- Extensive experiments on the benchmark dataset exhibit clear improvements of our method over SOTAs, in terms of both the overall glass detection accuracy and boundary clearness.

2. Related Work

In the past two years, glass detection began to attract attention but little work has been done on this topic. In this section, we briefly introduce the methods used in glass detection and the methods that can assist to solve this problem from relevant fields, including semantic segmentation, salient object detection, and mirror detection.

Semantic segmentation. Semantic segmentation is a key problem in the computer vision community, which aims at assigning semantic class labels to each pixel in the given image. With the development of deep neural networks, an end-to-end training architecture method, called fully convolutional networks (FCNs) [LSD15], is proposed, which uses multi-scale context fusion to achieve a high segmentation performance. However, the fixed geometric structures of convolution operation make the pixel capture local information and short-range contextual information inherently. Chen et al. [CPK*18] introduce an atrous spatial pyramid pooling module (ASPP) with multi-scale dilation convolutions for contextual information aggregation. Zhao et al. [ZSQ*17] further propose PSPNet to capture a wider range of contextual information by using a pooling operation and the pyramid structure. In addition, the encoder-decoder structures, like U-Net [RFB15], are widely used to fuse middle-level and high-level semantic features.

However, the dilated convolution-based methods [DJS*18, CPSA17] fails to capture global contextual information and causes sparse local information due to its structure, and the pool-based methods [ZDS*18, ZTZ*17] aggregates context information in a non-adaptive way to make image pixels use the homogeneous contextual information. Therefore, Wang et al. [WGGH18] introduce Non-local Networks utilizing self-attention mechanism [VSP*17, CDL16], which calculates the relationship between each pixel and all other pixels in the image, thus harvesting global contextual information. Huang et al. [HWH*19] and Fu et al. [FLT*19] respectively propose CCNet and DANet to solve the problem that self-attention based methods have high computation complexity and occupy a huge amount of GPU memory. Carion et al. [CMS*20] adopt Transformer that is widely used in the NLP field, which re-

places the convolution layer with the self-attention layer, for semantic segmentation.

Salient object detection(SOD). SOD aims at identifying the most visually distinctive objects or regions in an image, which is widely applied as a pre-processing procedure for the downstream tasks [XWL*18, WLF*21]. Early salient object detection methods are mainly based on hand-crafted features (e.g., color, texture, and contrast) to segment salient objects in the scene [YZL*13, ZLWS14, SB15, ZSL*15]. Recent Convolutional Neural Networks (CNNs) [KSH12, SZ14, HZRS16] are extensively used and achieve very remarkable performance.

Ronneberger et al. [RFB15] propose U-Net, a representative network widely used in a variety of graphics processing tasks, which effectively generates more accurate detection results by using a skip connection operation and an encoder-decoder structure. Many other methods, similar to UNet, but adopting different decoders combined with multi-level CNN features, have achieved remarkable performance. Zhang et al. [ZWL*17] introduce an AmuletNet aggregating an another-level convolutional feature at each different level for salient object detection. Zhang et al. [ZWQ*18] add an attention module to the decoder which can guide the network to selectively integrate multi-level features. Zhao et al. [ZW19] propose a pyramid feature attention network (PFAN) to enhance the high-level context features and the low-level spatial structural features. Pang et al. [PZZL20] propose aggregate interaction modules to integrate the features from adjacent levels, by using a more complex decoder structure. Besides, more efforts utilize boundary information to improve the accuracy of saliency maps. Zhao et al. [ZLF*19] focus on the complementarity between salient edge information and salient object information and present an edge guidance network (EGNet) for salient object detection. Zhou et al. [ZXL*20] analyze the correlation between saliency and boundary and introduce an interactive two-stream decoder to explore multiple cues, including saliency, boundary, and their correlation. Furthermore, Wei et al. [WWW*20] propose a label decoupling framework (LDF) that exploits more boundary information to enhance salient object detection performance.

Mirror detection. Similar to other image detection tasks, mirror detection aims at segmenting mirror regions in single images. Yang et al. [YMX*19] make the first attempt to automatically detect mirrors and propose MirrorNet by utilizing inconsistency between inside and outside of the mirror region, called contextual contrasted features, to segment mirrors from the real scene. The different performance between the mirror region that reflects the scene in front of the mirror and other non-mirror regions make the semantic and low-level discontinuities often occur at the boundary of the mirror. But not all mirrors have a great distinction between inside and outside. It exits little contextual contrasted information, thus, Lin et al. [LWL20] introduce a model to progressively learn the content similarity between the inside and outside of the mirror, while explicitly detecting the mirror boundaries. The scenes reflected by a mirror often exhibit similarities to scenes outside the mirror, which can aid to detect mirror regions by enlarging the receptive fields of the convolution operation. Glass detection is very similar to mirror detection that also has the problem of similar foreground and background.

Glass detection. Glass regions in an image do not have a fixed pattern, since they depends on what appears behind the glass, and the content of the glass region is the content of the background region. This situation makes it difficult to distinguish between the glass and the background region, even using state-of-the-art segmentation methods. Meanwhile, other object detection methods are also not suitable for glass detection tasks on account of the difference between both glass and other objects. Mei et al. [MYW*20] pioneer to propose a novel glass detection network (GDNet) by exploring abundant contextual features from a large receptive field. They utilize multiple well-designed large-field contextual feature integration modules to the precise positioning of the glass region, but this method has poor performance in some cases where the glass boundary region or scene is very complex or the background inside and outside the glass is insufficient. Lin et al. [LHL21] observe that humans often rely on identifying reflections to sense the existence of glass, and rely on locating the boundary in order to determine the extent of the glass. They propose a rich context aggregation module (RCAM) to extract multi-scale boundary features and a reflection-based refinement module (RRM) to detect reflection. Then, they utilize two modules for glass surface detection to solve the problem of insufficient contexts in part of the scene.

Transparent object detection(TOD). Similar to glass detection, transparent object detection (TOD) aims to segment transparent objects in single images. Xie et al. [XWW*20] propose a large-scale dataset for TOD named Trans10K, and a novel boundary-aware segmentation method termed TransLab to address the transparent object detection problem. However, there exists a difference between TOD and GD: TOD is a multi-label segmentation problem while GD is a binary segmentation problem. This fact indicates that TOD does not operate smoothly on the GD task, and vice versa. This is why we do not compare our method with those TOD methods.

3. Methodology

Motivation. Due to the unbalanced distribution between boundary pixels and background pixels, only using boundary pixels for glass detection will lead to larger prediction errors of pixels close to the boundary than those far away from the glass. Therefore, the glass boundary should diffuse itself into the glass's interior to amplify its influence. Conversely, the glass's interior should diffuse itself from center to boundary to loosen its influence. Based on this observation, we propose to decouple the glass label into the interior-diffusion part and the boundary-diffusion part, both of which are auxiliary supervisions to enhance the overall glass detection quality and boundary clearness. To make full use of the decoupled supervisions, we further present a three-stream network, which consists of the proposed multi-scale interactive dilation modules to effectively integrate large-field contextual features for detecting glass of different sizes. Also, our proposed network learns to fuse multi-modal information to further enhance the performance.

3.1. Label Decoupling

Many object detection methods pay attention to boundary information for the enhancement of detection accuracy, but the prediction

difficulty of boundary pixels is closely related to their locations. Therefore, it is difficult to classify the pixels near the boundary correctly, which is called hard examples [CZXL19]. In contrast, the consistency of interior regions makes the central region easier to be detected. Therefore, a strategy of dealing with boundary pixels and interior pixels differently will make detection results more reasonable. However, it is difficult to claim which pixels are hard examples or not, as illustrated in Figure 2. We adopt the label decoupling (LD) strategy proposed by Wang et al. [ZLF*19] to decouple the original glass map into an interior-diffusion map and a boundary-diffusion map, as shown in Figure 3. In detail, LD uses the simple Distance Transformation (DT) to convert the ground-truth glass map into a new image, where the value of the foreground pixel is the minimum distance from the background obtained by the distance function. Please note that the foreground herein refers to the glass region, and the background means the remaining non-glass region.

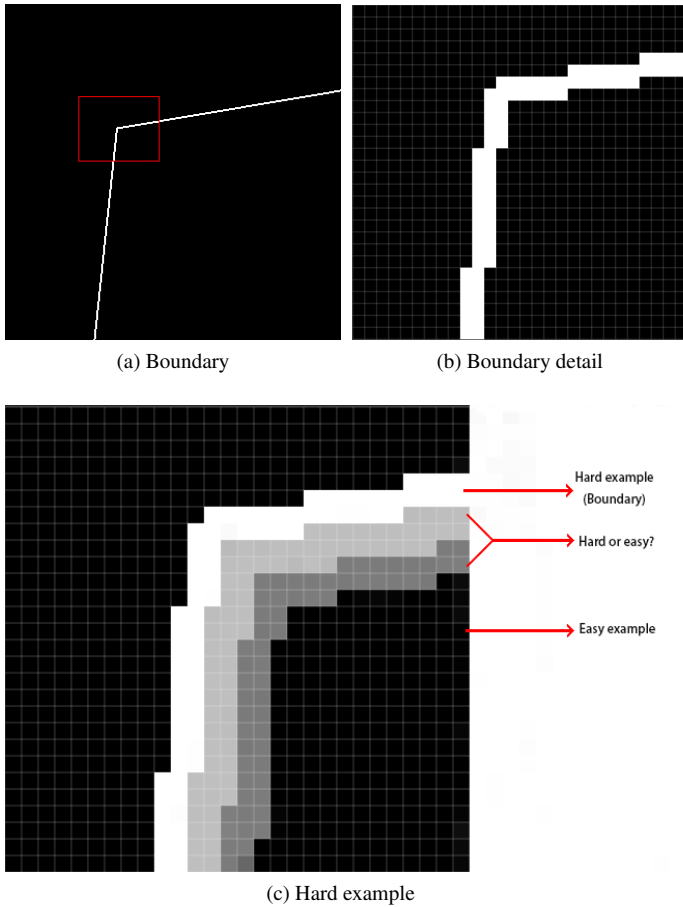


Figure 2: Illustration of hard examples. (a) the boundary obtained by the boundary extraction algorithm in EGNNet [ZLF*19], (b) boundary detail which is only two pixels wide, (c) It is challenging to determine pixels near the boundary to be hard examples or not.

Distance Transformation (DT) calculates the distance from the

nearest zero points to itself for each non-zero point in an image, so its input is a binary graph such as ground-truth of the image detection task, which can be divided into two groups (i.e., foreground I_{fg} and background I_{bg}). The original metric function is defined as $f(p, q) = \sqrt{(p_x - q_x)^2 + (p_y - q_y)^2}$ to calculate the distance between pixels, and here we modify it to fit our approach. The new distance function can be expressed as:

$$I'(p) = \begin{cases} \min_{q \in I_{bg}} f(p, q), & p \in I_{fg} \\ 0, & p \in I_{bg} \end{cases} \quad (1)$$

For the foreground pixel p , DT calculates the original distance function $f(p, q)$ by looking for its nearest pixel q in the background pixel, and directly sets the value to 0 for the background pixel. We use a linear function $I' = \frac{I' - \min(I')}{\max(I') - \min(I')}$ that can normalize the image generated from the new distance function to map the original value to $[0, 1]$. Compared with the original image, the new image obtained by defining the distance function depends not only on its foreground or the background but also on its relative position. Therefore, the new image corresponds to the inner part of the original image, and the closer to the center, the larger the pixel value. Boundary images obtained by subtracting the new image from the original image can help us deal with hard examples. To remove background interference, we processed the new image and the original ground-truth to generate the interior-diffusion label and boundary-diffusion label:

$$Label \Rightarrow \begin{cases} BL = I * I' \\ DL = I * (1 - I') \end{cases} \quad (2)$$

where BL means the interior-diffusion label and DL represents the boundary-diffusion label. So we decoupled the original tag into two different kinds of labels, to assist the network to learn inner and boundary features with different characteristics respectively.

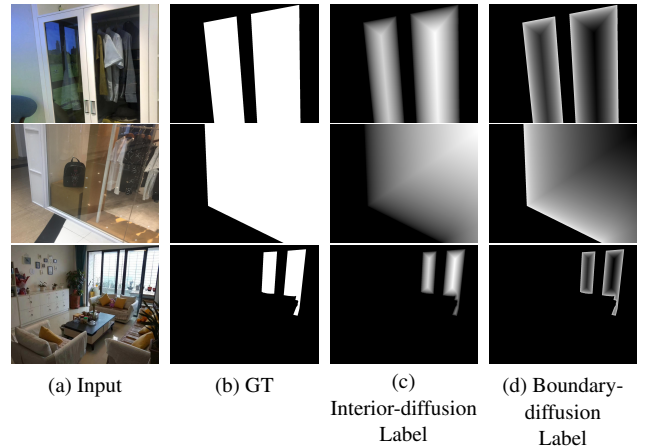


Figure 3: Examples of label decoupling. (c) represents the interior-diffusion label of the ground truth, where pixels close to the center of the target have larger values. (d) means the boundary-diffusion label of the ground truth, where pixels near the boundary of the target have larger values. The sum of (c) and (d) is equal to (b).

3.2. Network Overview

The overview of the proposed model is illustrated in Figure 4, which is composed of three parallel streams: interior-diffusion stream, boundary-diffusion stream, and glass stream. We first feed an image to the backbone network to extract multi-scale backbone features. Then, the features of each level are fed into the three streams supervised by the decoupled labels to generate different features respectively. In each stream, we use Multi-scale Interactive Dilation Module (MID) to extract large-field contextual features, then obtain the glass features, interior-diffusion features, and boundary-diffusion features under each stream. Finally, we use the attention-based Boundary-aware Feature Mosaic Module (BFM) to integrate the boundary features and interior-diffusion features into the glass prediction maps to generate the final glass map of the whole network. Details of the proposed approach are described as follows.

Feature encoder. We use ResNet-50 [HZRS16] as the backbone network to extract common multi-level image features for three streams as suggested by [WBZ*17, WZW*18, LHY18]. In particular, as a backbone network, we remove the last global pooling and fully connected layers and use only the five residual blocks. For the sake of simplification, we represent this five block as $f_i(w_i), i \in \{1, \dots, 5\}$, where w_i is the weight parameters pre-trained on ImageNet [DDS*09] of $f_i(\cdot)$ operation, and the output of i -th layer $f_i(\cdot)$ is the input of $f_{i+1}(\cdot), \forall i \in \{1, \dots, 4\}$. We feed an input image with shape $H \times W$ into it to generate different scale feature denoted as $EF = \{EF_i | i = 1, 2, 3, 4, 5\}$ by utilizing $f_i(w_i), i \in \{1, \dots, 5\}$, eg. $EF_{i+1} = f_i(EF_i)$. The size of the i -th feature is $\frac{W_i}{2^i} \times \frac{H_i}{2^i} \times C_i$, where C_i is the channel of the i -th feature. The feature EF_5 and EF_4 is feed into interior-diffusion stream decoder to roughly locate the glass region. And we input the feature $\{EF_i | i = 1, 2, 5\}$ to boundary-diffusion stream decoder to obtain a finer glass boundary. In addition, we utilize all features for glass map generation in glass stream.

Three-stream decoder. As shown in Figure 4, we built a three-stream network to use label decoupling information. We utilize a label decoupling procedure to decompose a glass label into an interior-diffusion map and boundary-diffusion map to supervise the model separately. Through the supervision of these three different labels, better detection results can be obtained.

In each stream, we use a Multi-scale Interactive Dilation Module (MID) to extract large-field contextual features. Figure 4 illustrates the detailed structure of the Decoder. For the glass stream and boundary-diffusion stream, we employ the short connections [HCH*17] to merge feature maps EF_i at different CNN layers, resulting in new feature maps (denoted as DF_i). Specifically, the merged feature map DF_i at the k -th CNN layer ($i = 1, \dots, 5$) is computed by

$$DF_i = \text{Conv}(\text{Concat}(MF_i, \dots, MF_5)) \quad (3)$$

Then we use the MID to generate large-field contextual features MF_i , which can be formulated as:

$$MF_i = \text{MID}(DF_i) \quad (4)$$

where $\text{MID}(\cdot)$ is the Multi-scale Interactive Dilation Module. Then we integrate the different levels of MF by a decoder structure. In

particular, we concatenate the output of each level in the boundary-diffusion stream to get the final boundary map. For the interior-diffusion stream, we add EF_4 and EF_5 by using the element-wise addition operation and input it into MID to generate MF. In this way, different level feature maps are jointly fused, which is beneficial for semantic segmentation.

3.3. Multi-scale Interactive Dilation Module

For glass detection, the key to accurately locate glass regions is to aggregate a wide range of contextual features at different scales. To enhance such capability, we propose a multi-scale interactive dilation module (named as MID, as shown in Figure 5) to efficiently aggregate contextual information at a sequence of scales for the purpose of enhancing the performance of glass detection.

To address this issue, we consider using a wide range of contextual information and propose to utilize a dilated convolution with different dilation rates to expand the receiving field of each pixel so that it can obtain a wider range of contextual information. After entering the feature map into this module, these maps first pass through a convolution layer for feature extraction at each of the branches. Then we use dilated convolution with dilation rate being set to 2, 4, 8, 16 respectively to extract a wide range of context features. Meanwhile, we adopt Short Connections [HCH*17] having proved its effectiveness in some typical networks such as ResNet and U-Net to transfer the output of the smaller receiving field branch into the other larger branch for getting more contextual information. Finally, we integrate the context feature maps of each branch through convolution layers and obtain the feature map MF utilizing element-wise addition operation.

3.4. Attention-based Boundary-aware Feature Mosaic Module

After obtaining a high-quality boundary prediction map by using boundary-diffusion stream, we utilize a Boundary-aware Feature Mosaic Module (BFM) to integrate the boundary maps into the predicted glass maps generated by the glass stream, as Figure 6 showed. BFM first takes the predicted boundary map, interior-diffusion map, and glass feature map as input feature. Through using the predicted boundary map and the interior-diffusion map as attention maps, we integrate them into the feature maps of the glass stream by using an element-wise product operation \otimes . We concatenate the interior-diffusion map and boundary map obtained by the above procedure and input them into the SE module respectively to enhance the corresponding boundary and interior-diffusion features. **Here the SE module is an architectural unit proposed by Hu et al. [HSS18], which is termed as the ‘‘Squeeze-and-Excitation’’ (SE) block, that adaptively recalibrates channel-wise feature responses by explicitly modelling interdependencies between channels.** Finally, we add the enhanced features to the input glass feature map to generate the final output.

3.5. Loss Function

For three-stream supervised by different labels, we also need to use different loss functions that are three types of losses, binary cross-entropy (BCE) loss l_{bce} , IoU loss l_{iou} [QZH*19] and Dice loss l_{dice} [MNA16], to optimize the network.

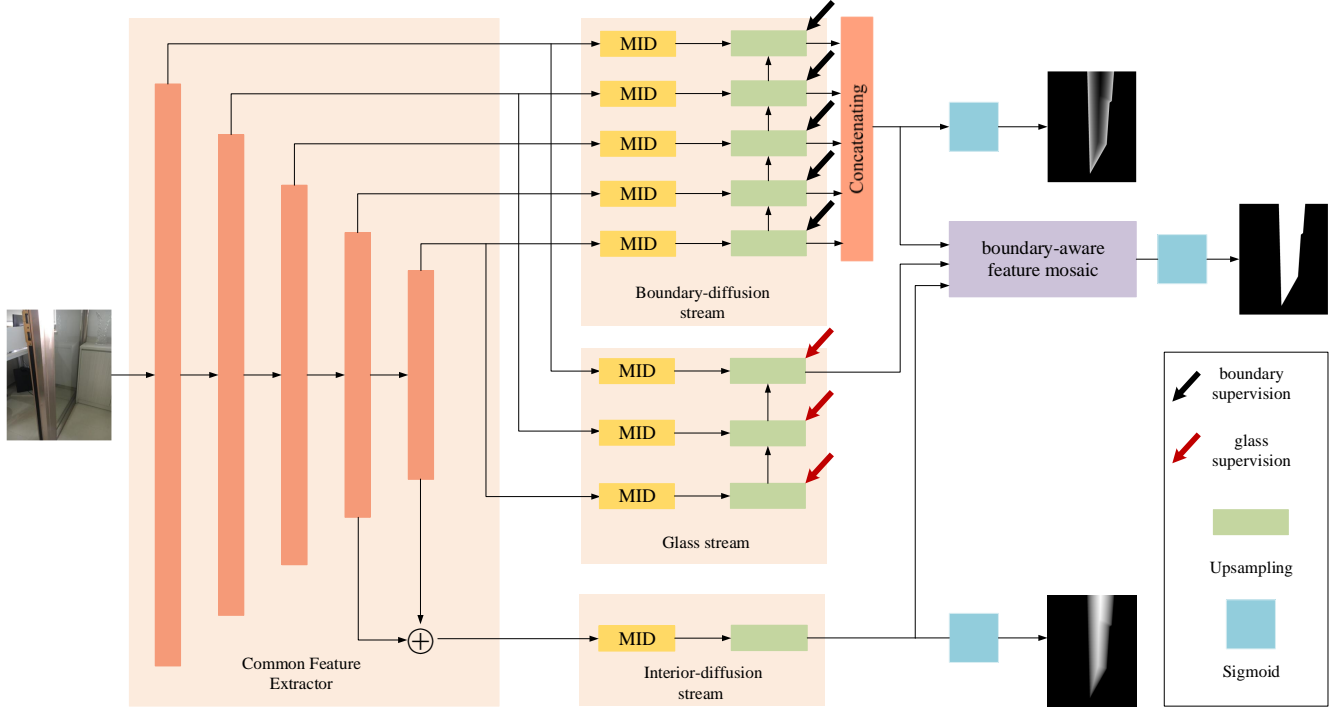


Figure 4: Overview of the proposed network. The pre-trained ResNet-50 [HZRS16] is employed as the backbone network to extract common multi-level image features. The extracted image features are fed into three streams. In each of the three streams, we use Multi-scale Interactive Dilation Module (MID) to extract large-field contextual features, to obtain glass features, interior-diffusion features, and boundary-diffusion features respectively through supervision. The three different features are fused through an attention-based Boundary-aware Feature Mosaic Module (BFM) and fed themselves into the predict block to generate the final glass map.

BCE loss is a widely used loss function in the computer vision task due to its robustness:

$$l_{bce} = - \sum_{(x,y)} [g(x,y) \log(p(x,y)) + (1 - g(x,y)) \log(1 - p(x,y))] \quad (5)$$

IoU, Intersection over Union, is an important metric to evaluate object detection results by calculating the ratio of the intersection and union of "predicted box" and "GT box" in the beginning. Recently, it is widely used as the training loss:

$$l_{iou} = 1 - \frac{\sum_{x=1}^H \sum_{y=1}^W p(x,y)g(x,y)}{\sum_{y=1}^W \sum_{x=1}^H [p(x,y) + g(x,y) - p(x,y)g(x,y)]} \quad (6)$$

Similar to IOU, Dice is a measure to measure the similarity between two sets. The proposal of Dice Loss is to solve the problem that the foreground is too small, so we utilize it to calculate the loss at the boundary. The dice coefficient $D(p(x,y), g(x,y))$ and Dice

loss are formulated as follow:

$$D(p(x,y), g(x,y)) = \frac{2 \sum_{x=1}^H \sum_{y=1}^W p(x,y)g(x,y)}{\sum_{y=1}^W \sum_{x=1}^H [p(x,y) + g(x,y) - p(x,y)g(x,y)]} \quad (7)$$

$$l_{dice} = 1 - D(p(x,y), g(x,y)) \quad (8)$$

where $g(x,y) \in [0, 1]$ is the ground truth label of the pixel (x,y) and $p(x,y) \in [0, 1]$ is the predicted probability of being glass.

In the interior-diffusion stream, the glass stream, and the final output prediction maps, we adopt BCE loss and IoU loss which can be formulated as:

$$L_{glass} = \sum_{k=1}^{N_g} [l_{bce}(p_k, g_{glass}) + l_{iou}(p_k, g_{glass})] \quad (9)$$

$$L_{inner} = l_{bce}(p_k, g_{inner}) + l_{iou}(p_k, g_{inner}) \quad (10)$$

$$L_{final} = l_{bce}(p_k, g_{glass}) + l_{iou}(p_k, g_{glass}) \quad (11)$$

where p_k is the prediction maps of the different branches in three-

Algorithm	CRF	acc \uparrow	IoU \uparrow	$F_{\beta}\uparrow$	MAE \downarrow	BER \downarrow
PSPNet [ZSQ*17]	×	0.916	0.841	0.906	0.084	8.79
DenseASPP [YYZ*18]	×	0.919	0.837	0.911	0.081	8.66
PSANet [ZZL*18]	×	0.918	0.835	0.909	0.082	9.09
CCNet [HWH*19]	×	0.915	0.843	0.904	0.085	8.63
DANet [FLT*19]	×	0.911	0.842	0.901	0.089	8.96
R ³ Net [DHZ*18]	✓	0.869	0.767	0.869	0.132	13.85
CPD [WSH19]	×	0.907	0.825	0.903	0.095	8.87
BASNet [QZH*19]	×	0.907	0.829	0.896	0.094	8.70
EGNet [ZLF*19]	×	0.885	0.788	0.858	0.115	10.87
LDF [WWW*20]	×	0.921	0.843	0.908	0.079	7.52
BDRAR [ZDH*18]	✓	0.902	0.800	0.908	0.098	9.87
DSC [HZF*18]	×	0.914	0.836	0.911	0.090	7.97
MirrorNet [YMX*19]	✓	0.918	0.851	0.903	0.083	7.67
PMD [LWL20]	✓	0.921	0.836	0.894	0.078	8.34
GDNet [MYW*20]	×	0.939	0.876	0.920	0.061	5.62
GlassNet (ours)	×	0.946	0.887	0.937	0.054	5.42

Table 1: Quantitative results on the GDD dataset. CRF indicates whether CRFs [KK11] is used for post-processing. The first, second, and third best results are marked in bold, red, and blue, respectively.

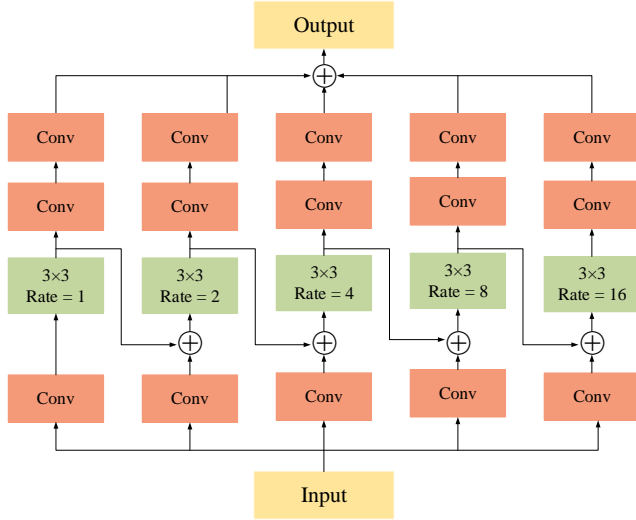


Figure 5: Structure of the Multi-scale Interactive Dilation (MID) module. *Conv* represents a convolutional layer with a kernel size of 3×3 , a normalized layer, and a ReLU layer. 3×3 means the convolutional kernel size, and Rate represents the dilation rate in dilated convolution.

stream. g_{glass} is the ground-truth label and g_{inner} is the interior-diffusion label decoupled by the original label. N_i and N_g are the numbers of branches in the interior-diffusion stream and the glass stream, respectively. Moreover, BCE loss and Dice loss are used in the boundary-diffusion stream.

$$L_{boundary} = \sum_{k=1}^{N_b} [l_{bce}(p_k, g_{boundary}) + l_{Dice}(p_k, g_{boundary})] \quad (12)$$

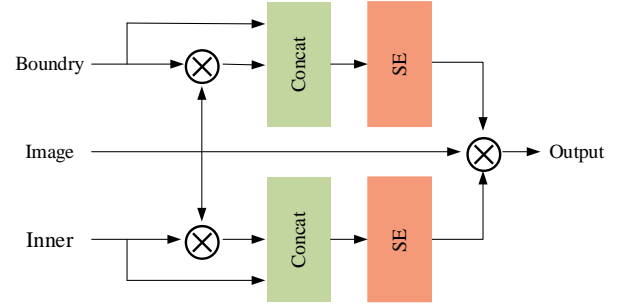


Figure 6: Attention-based boundary-aware feature Mosaic module.

where $g_{boundary}$ is the boundary-diffusion label decoupled by the original label and N_b are the number of branches in the boundary-diffusion stream.

The final loss function is:

$$Loss = \alpha L_{inner} + \beta L_{boundary} + L_{glass} + L_{final} \quad (13)$$

where α and β represent a trade-off between different streams, and are all set to 1 by default in our experiments.

4. Experiments

4.1. Datasets and Evaluation Metrics

Currently, there is a dataset available, i.e. GDD [MYW*20], which is the first large-scale benchmark specifically for glass detection and has 4,018 mirror images with corresponding masks. To evaluate the works, we use five metrics widely adopted by other computer vision tasks to evaluate the performance of our model and existing state-of-the-art methods. First, we use two popular met-

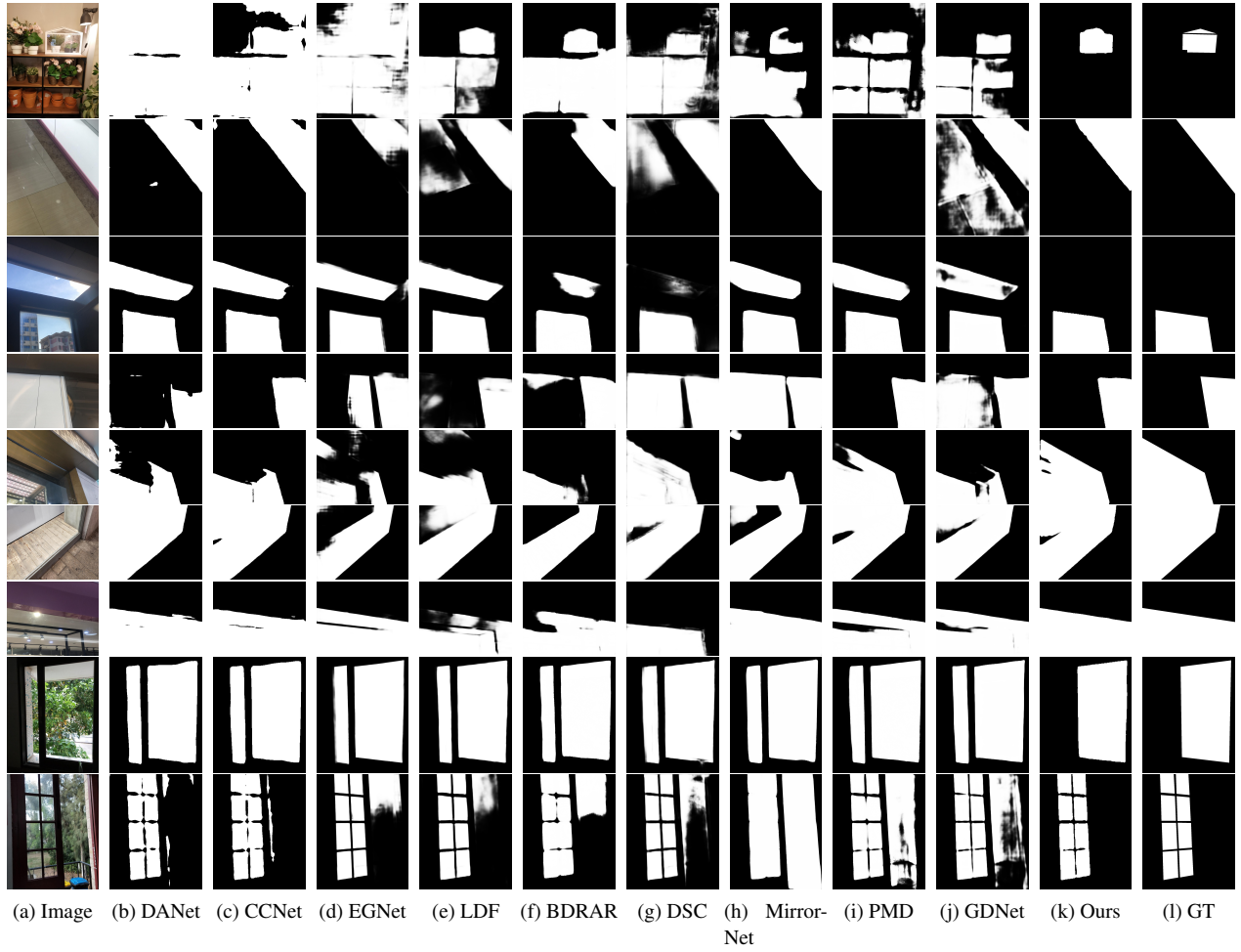


Figure 7: Visual comparison of our network to the state-of-the-art methods on the GDD test set.

strategy	acc \uparrow	$F_{\beta}\uparrow$	BER \downarrow
w/o interior and boundary	0.936	0.925	6.37
w/o boundary	0.938	0.927	6.25
w/o interior	0.941	0.932	5.98
w/ only bce loss	0.937	0.928	6.31
w/o iou loss	0.940	0.933	5.92
w/o dice loss	0.938	0.930	6.22
w/o MID	0.943	0.932	5.53
w/o BFM	0.940	0.923	5.80
Our GlassNet	0.946	0.937	5.42

Table 2: Ablation study results. Best results are highlighted in bold.

rics, pixel accuracy (acc) and the intersection of union (IoU). Besides we apply the F-measure [AHES09] and mean absolute error (MAE) metrics from the salient object detection field, which is widely adopted in [CTWH18, LYC*18, LHY18, HCH*17]. F-measure is the weighted harmonic mean of precision and recall that

can be calculated by:

$$F_{\beta} = \frac{(1 + \beta^2) \text{Precision} \times \text{Recall}}{\beta^2 \text{Precision} + \text{Recall}} \quad (14)$$

where β^2 is set to 0.3 as shown in [AHES09]. MAE is mean absolute error, e.g. the mean value of the absolute error between the prediction and the ground-truth, which is defined as:

$$MAE = \frac{1}{H \times W} \sum_{i=1}^H \sum_{j=1}^W |p(i, j) - g(i, j)| \quad (15)$$

where $g(x, y) \in [0, 1]$ is the ground truth label of the pixel (x, y) and $p(x, y) \in [0, 1]$ is the predicted probability of being glass. In addition, we select the balance error rate (BER) [VHS15] from the shadow detection field as our last metric, which can be obtained by following way:

$$BER = 100 \times \left(1 - \frac{1}{2} \left(\frac{TP}{N_p} + \frac{TN}{N_n} \right) \right) \quad (16)$$

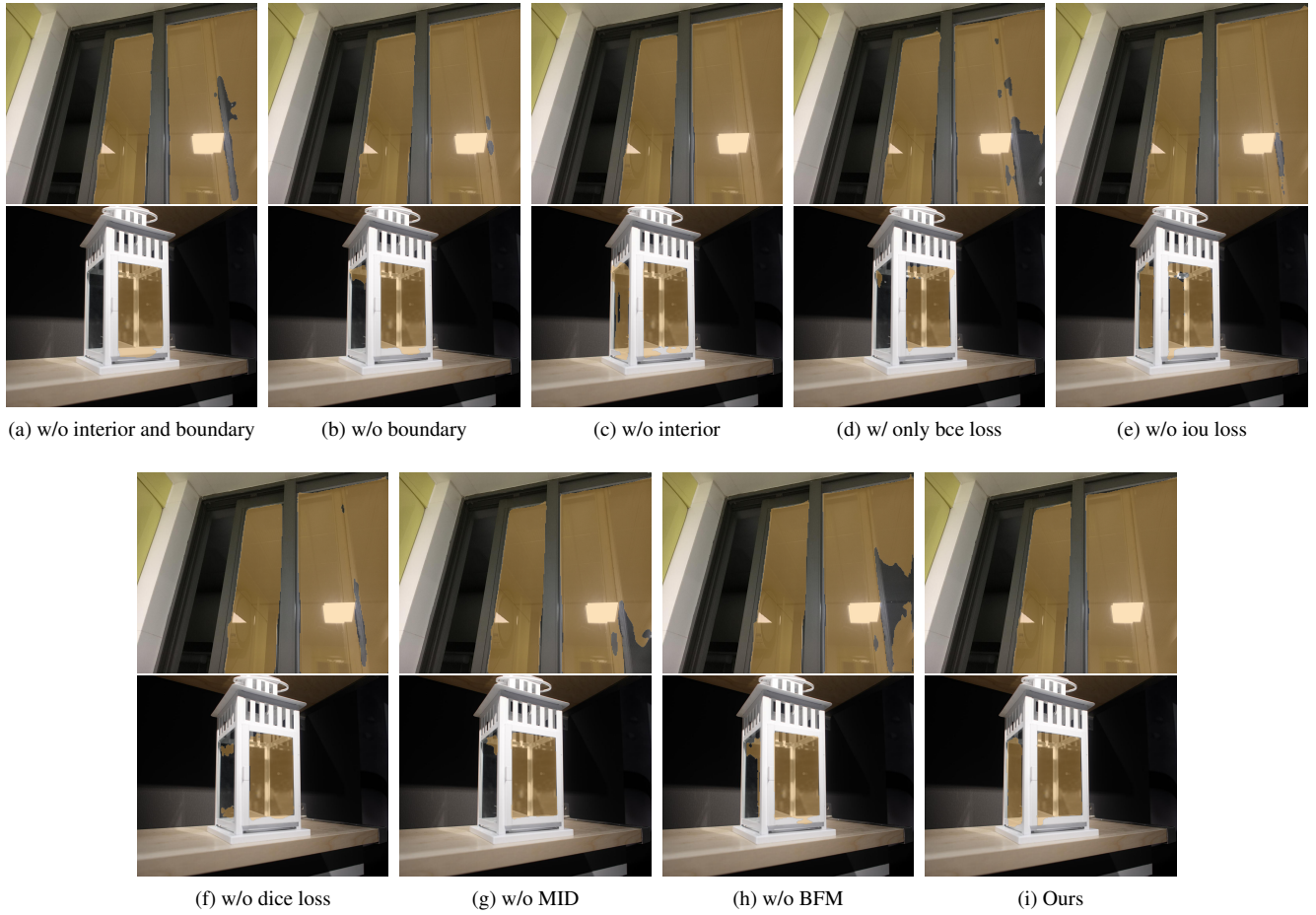


Figure 8: Visual comparison of our method with variations.

where TP , TN , N_n and N_p is the numbers of true positives, true negatives, glass pixels and non-glass pixels, respectively.

4.2. Implementation Details

We use the PyTorch framework [PGM*19] to implement the proposed network BLDNet trained on benchmark dataset GDD. We utilize horizontal flip, random crop and multi-scale input images to augment data. We use the pre-trained ResNet-50 network [HZRS16] on ImageNet [DDS*09] to initialize the parameters of backbone and the other parameters are initialized randomly. Training the whole network by using stochastic gradient descent (SGD) with a momentum of 0.9 and weight decay of 5×10^{-4} . The initial learning rate is set to 0.0001 for ResNet-50 backbone and 0.001 for other parts and is adjusted by warm-up and poly decay strategies [YWP*18] with a power of 0.9. The network with the batch setting of 4 is trained on an NVIDIA GTX 1080 Ti graphics card. During testing, images are adjusted to the resolution of 512×512 for inference without any post-processing.

4.3. Comparison with the SOTAs

Compared methods. There's only one way for glass detection from a single image in deep learning, so we use this method and other 14 state-of-the-art methods, which are PSPNet [ZSQ*17], DenseASPP [YYZ*18], PSANet [ZZL*18], DANet [FLT*19] and CCNet [HWH*19] chosen from the semantic segmentation field, R³Net [DHZ*18], CPD [WSH19], BASNet [QZH*19], EG-Net [ZLF*19] and LDF [WWW*20] chosen from the salient object detection field, DSC [HZF*18] and BDRAR [ZDH*18] chosen from the shadow detection field, MirrorNet [YMX*19] and PMD [LWL20] from the mirror segmentation field, and GDNet [MYW*20] used for glass detection. For a fair comparison, we re-trained other methods on the GDD dataset by using their publicly available codes.

Quantitative Comparison. We will compare the proposed network with state-of-the-art methods from the relevant fields mentioned above, which are shown in Table 1. The first, second, and third best results are marked in bold, red, and blue, respectively. Obviously, compared with other methods in related fields, our method is obviously better than the SOTA methods.

Qualitative Evaluation. Some prediction examples of the proposed method and other state-of-the-art approaches have been shown in Figure 7. We observe that the proposed method not only highlights the glass regions clearly but also well suppresses the background noises. It can be seen that our method can accurately detect small glass (e.g., the first four rows), large glass (e.g., the fifth to seventh rows), and others (e.g., eighth and ninth rows). Although GDNet can also locate these regions well, it has low detection accuracy for the boundary regions and even cannot detect the boundary regions correctly. In contrast, our method has higher detection accuracy in the boundary region, because we use boundary information to force the network to pay more attention to the boundary region.



Figure 9: Failure cases.

4.4. Ablation Studies

Table 2 demonstrates the effectiveness of each component in our model. From the first lines to the third line, we can see that boundary and interior-diffusion branches can effectively improve the performance. Moreover, the effect of the network without the boundary-diffusion stream is worse than that without the interior-diffusion stream, which is consistent with our observation: Boundaries significantly improve the detection ability, which should be specially considered. In addition, the final detection accuracy can also be improved for the multiple mixing losses we proposed, as shown in the 4th to 6th lines, where each row will omit a loss,

i.e., BCE, IOU, and DICE, respectively. Finally, w/o MID and w/o BFM respectively indicate that we do not use any one of the two modules each time in our network, which show their contributions on improving the glass detection quality. Figure 8 shows a visual example, proving that our method successfully addresses the glass segmentation problem with the help of boundaries.

4.5. Failure cases

Our proposed network has at least two limitations as shown in Figure 9. In the case of very large-scale glasses, e.g., the area of glass occupies more than 95 percent or even 100 percent of the whole image, our network may operate poorly on such extreme cases, due to the lack of sufficient contextual information. In addition, under the very weak-light condition, the boundary area of the glass and the background will share very similar properties, i.e., they are all black regions with pixel values approximating to (0,0,0). Thus, it is nearly impossible to detect the glass in the very weak light.

5. Conclusion

In this paper, we have proposed a three-stream network for glass detection in a single image. The method consists of a label decoupling procedure that can decouple ground-truth into interior-diffusion label and boundary-diffusion label, a multi-scale interactive dilation module for extracting and capturing contextual features for glass detection, and a three-stream network integrating multi-scale and multi-modal information to generate the final prediction map. Besides, the proposed network utilizes an attention-based boundary-aware feature mosaic module to integrate multi-modal information for further improving the glass detection effect. Experiments on benchmark dataset demonstrate that the proposed method outperforms the state-of-the-art method under different evaluation metrics.

References

- [AHES09] ACHANTA R., HEMAMI S., ESTRADA F., SUSSTRUNK S.: Frequency-tuned salient region detection. In *2009 IEEE conference on computer vision and pattern recognition* (2009), IEEE, pp. 1597–1604.
- [CDL16] CHENG J., DONG L., LAPATA M.: Long short-term memory-networks for machine reading. *arXiv preprint arXiv:1601.06733* (2016).
- [CMS*20] CARION N., MASSA F., SYNNAEVE G., USUNIER N., KIRILLOV A., ZAGORUYKO S.: End-to-end object detection with transformers. In *European Conference on Computer Vision* (2020), Springer, pp. 213–229.
- [CPK*18] CHEN L.-C., PAPANDREOU G., KOKKINOS I., MURPHY K., YUILLE A. L.: Deeplab: Semantic image segmentation with deep convolutional nets, atrous convolution, and fully connected crfs. *IEEE Transactions on Pattern Analysis and Machine Intelligence* 40, 4 (2018), 834–848. doi:10.1109/TPAMI.2017.2699184.
- [CPSA17] CHEN L.-C., PAPANDREOU G., SCHROFF F., ADAM H.: Re-thinking atrous convolution for semantic image segmentation. *arXiv preprint arXiv:1706.05587* (2017).
- [CTWH18] CHEN S., TAN X., WANG B., HU X.: Reverse attention for salient object detection. In *Proceedings of the European Conference on Computer Vision (ECCV)* (2018), pp. 234–250.

- [CZXL19] CHEN Z., ZHOU H., XIE X., LAI J.: Contour loss: Boundary-aware learning for salient object segmentation. *arXiv preprint arXiv:1908.01975* (2019).
- [DDS*09] DENG J., DONG W., SOCHER R., LI L.-J., LI K., FEI-FEI L.: Imagenet: A large-scale hierarchical image database. In *2009 IEEE conference on computer vision and pattern recognition* (2009), Ieee, pp. 248–255.
- [DHZ*18] DENG Z., HU X., ZHU L., XU X., QIN J., HAN G., HENG P.-A.: R3net: Recurrent residual refinement network for saliency detection. In *Proceedings of the 27th International Joint Conference on Artificial Intelligence* (2018), AAAI Press, pp. 684–690.
- [DJS*18] DING H., JIANG X., SHUAI B., LIU A. Q., WANG G.: Context contrasted feature and gated multi-scale aggregation for scene segmentation. In *Proceedings of the IEEE Conference on Computer Vision and Pattern Recognition* (2018), pp. 2393–2402.
- [FLT*19] FU J., LIU J., TIAN H., LI Y., BAO Y., FANG Z., LU H.: Dual attention network for scene segmentation. In *Proceedings of the IEEE/CVF Conference on Computer Vision and Pattern Recognition* (2019), pp. 3146–3154.
- [HCH*17] HOU Q., CHENG M.-M., HU X., BORJI A., TU Z., TORR P. H.: Deeply supervised salient object detection with short connections. In *Proceedings of the IEEE conference on computer vision and pattern recognition* (2017), pp. 3203–3212.
- [HSS18] HU J., SHEN L., SUN G.: Squeeze-and-excitation networks. In *Proceedings of the IEEE conference on computer vision and pattern recognition* (2018), pp. 7132–7141.
- [HWH*19] HUANG Z., WANG X., HUANG L., HUANG C., WEI Y., LIU W.: Ccnet: Criss-cross attention for semantic segmentation. In *Proceedings of the IEEE/CVF International Conference on Computer Vision* (2019), pp. 603–612.
- [HZF*18] HU X., ZHU L., FU C.-W., QIN J., HENG P.-A.: Direction-aware spatial context features for shadow detection. In *Proceedings of the IEEE Conference on Computer Vision and Pattern Recognition* (2018), pp. 7454–7462.
- [HZRS16] HE K., ZHANG X., REN S., SUN J.: Deep residual learning for image recognition. In *Proceedings of the IEEE conference on computer vision and pattern recognition* (2016), pp. 770–778.
- [KK11] KRÄHENBÜHL P., KOLTUN V.: Efficient inference in fully connected crfs with gaussian edge potentials. *Advances in neural information processing systems* 24 (2011), 109–117.
- [KSH12] KRIZHEVSKY A., SUTSKEVER I., HINTON G. E.: Imagenet classification with deep convolutional neural networks. *Advances in neural information processing systems* 25 (2012), 1097–1105.
- [LHL21] LIN J., HE Z., LAU R. W.: Rich context aggregation with reflection prior for glass surface detection. In *Proceedings of the IEEE/CVF Conference on Computer Vision and Pattern Recognition* (2021), pp. 13415–13424.
- [LHY18] LIU N., HAN J., YANG M.-H.: Picanet: Learning pixel-wise contextual attention for saliency detection. In *Proceedings of the IEEE Conference on Computer Vision and Pattern Recognition* (2018), pp. 3089–3098.
- [LSD15] LONG J., SHELHAMER E., DARRELL T.: Fully convolutional networks for semantic segmentation. In *Proceedings of the IEEE conference on computer vision and pattern recognition* (2015), Proceedings of the IEEE conference on computer vision and pattern recognition, pp. 3431–3440.
- [LWL20] LIN J., WANG G., LAU R. W.: Progressive mirror detection. In *Proceedings of the IEEE/CVF Conference on Computer Vision and Pattern Recognition* (2020), pp. 3697–3705.
- [LYC*18] LI X., YANG F., CHENG H., LIU W., SHEN D.: Contour knowledge transfer for salient object detection. In *Proceedings of the European Conference on Computer Vision (ECCV)* (2018), pp. 355–370.
- [MNA16] MILLETARI F., NAVAB N., AHMADI S.-A.: V-net: Fully convolutional neural networks for volumetric medical image segmentation. In *2016 fourth international conference on 3D vision (3DV)* (2016), IEEE, pp. 565–571.
- [MYW*20] MEI H., YANG X., WANG Y., LIU Y., HE S., ZHANG Q., WEI X., LAU R. W.: Don't hit me! glass detection in real-world scenes. In *Proceedings of the IEEE/CVF Conference on Computer Vision and Pattern Recognition* (2020), pp. 3687–3696.
- [PGM*19] PASZKE A., GROSS S., MASSA F., LERER A., BRADBURY J., CHANAN G., KILLEEN T., LIN Z., GIMELSHEIN N., ANTIGA L., ET AL.: Pytorch: An imperative style, high-performance deep learning library. *arXiv preprint arXiv:1912.01703* (2019).
- [PZZL20] PANG Y., ZHAO X., ZHANG L., LU H.: Multi-scale interactive network for salient object detection. In *Proceedings of the IEEE/CVF Conference on Computer Vision and Pattern Recognition* (2020), pp. 9413–9422.
- [QZH*19] QIN X., ZHANG Z., HUANG C., GAO C., DEGHAN M., JAGERSAND M.: Basnet: Boundary-aware salient object detection. In *Proceedings of the IEEE/CVF Conference on Computer Vision and Pattern Recognition* (2019), pp. 7479–7489.
- [RFB15] RONNEBERGER O., FISCHER P., BROX T.: U-net: Convolutional networks for biomedical image segmentation. In *International Conference on Medical image computing and computer-assisted intervention* (2015), Springer, pp. 234–241.
- [SB15] SRIVATSA R. S., BABU R. V.: Salient object detection via objectness measure. In *2015 IEEE International Conference on Image Processing (ICIP)* (2015), IEEE, pp. 4481–4485.
- [SZ14] SIMONYAN K., ZISSERMAN A.: Very deep convolutional networks for large-scale image recognition. *arXiv preprint arXiv:1409.1556* (2014).
- [VHS15] VICENTE T. F. Y., HOAI M., SAMARAS D.: Leave-one-out kernel optimization for shadow detection. In *Proceedings of the IEEE International Conference on Computer Vision* (2015), pp. 3388–3396.
- [VSP*17] VASWANI A., SHAZEER N., PARMAR N., USZKOREIT J., JONES L., GOMEZ A. N., KAISER Ł., POLOSUKHIN I.: Attention is all you need. *arXiv preprint arXiv:1706.03762* (2017).
- [WBZ*17] WANG T., BORJI A., ZHANG L., ZHANG P., LU H.: A stagewise refinement model for detecting salient objects in images. In *Proceedings of the IEEE International Conference on Computer Vision* (2017), pp. 4019–4028.
- [WGGH18] WANG X., GIRSHICK R., GUPTA A., HE K.: Non-local neural networks. In *Proceedings of the IEEE conference on computer vision and pattern recognition* (2018), pp. 7794–7803.
- [WLF*21] WANG W., LAI Q., FU H., SHEN J., LING H., YANG R.: Salient object detection in the deep learning era: An in-depth survey. *IEEE Transactions on Pattern Analysis and Machine Intelligence* (2021).
- [WSH19] WU Z., SU L., HUANG Q.: Cascaded partial decoder for fast and accurate salient object detection. In *Proceedings of the IEEE/CVF Conference on Computer Vision and Pattern Recognition* (2019), pp. 3907–3916.
- [WWW*20] WEI J., WANG S., WU Z., SU C., HUANG Q., TIAN Q.: Label decoupling framework for salient object detection. In *Proceedings of the IEEE/CVF Conference on Computer Vision and Pattern Recognition* (2020), pp. 13025–13034.
- [WZW*18] WANG T., ZHANG L., WANG S., LU H., YANG G., RUAN X., BORJI A.: Detect globally, refine locally: A novel approach to saliency detection. In *Proceedings of the IEEE conference on computer vision and pattern recognition* (2018), pp. 3127–3135.
- [XWL*18] XIN Y., WANG S., LI L., ZHANG W., HUANG Q.: Reverse densely connected feature pyramid network for object detection. In *Asian Conference on Computer Vision* (2018), Springer, pp. 530–545.
- [XWW*20] XIE E., WANG W., WANG W., DING M., SHEN C., LUO

- P.: Segmenting transparent objects in the wild. In *Computer Vision–ECCV 2020: 16th European Conference, Glasgow, UK, August 23–28, 2020, Proceedings, Part XIII 16* (2020), Springer, pp. 696–711.
- [YMX*19] YANG X., MEI H., XU K., WEI X., YIN B., LAU R. W.: Where is my mirror? In *Proceedings of the IEEE/CVF International Conference on Computer Vision* (2019), pp. 8809–8818.
- [YWP*18] YU C., WANG J., PENG C., GAO C., YU G., SANG N.: Bisenet: Bilateral segmentation network for real-time semantic segmentation. In *Proceedings of the European conference on computer vision (ECCV)* (2018), pp. 325–341.
- [YYZ*18] YANG M., YU K., ZHANG C., LI Z., YANG K.: Denseaspp for semantic segmentation in street scenes. In *Proceedings of the IEEE conference on computer vision and pattern recognition* (2018), pp. 3684–3692.
- [YZL*13] YANG C., ZHANG L., LU H., RUAN X., YANG M.-H.: Saliency detection via graph-based manifold ranking. In *Proceedings of the IEEE conference on computer vision and pattern recognition* (2013), pp. 3166–3173.
- [ZDH*18] ZHU L., DENG Z., HU X., FU C.-W., XU X., QIN J., HENG P.-A.: Bidirectional feature pyramid network with recurrent attention residual modules for shadow detection. In *Proceedings of the European Conference on Computer Vision (ECCV)* (2018), pp. 121–136.
- [ZDS*18] ZHANG H., DANA K., SHI J., ZHANG Z., WANG X., TYAGI A., AGRAWAL A.: Context encoding for semantic segmentation. In *Proceedings of the IEEE conference on Computer Vision and Pattern Recognition* (2018), pp. 7151–7160.
- [ZLF*19] ZHAO J.-X., LIU J.-J., FAN D.-P., CAO Y., YANG J., CHENG M.-M.: Egnnet: Edge guidance network for salient object detection. In *Proceedings of the IEEE/CVF International Conference on Computer Vision* (2019), pp. 8779–8788.
- [ZLWS14] ZHU W., LIANG S., WEI Y., SUN J.: Saliency optimization from robust background detection. In *Proceedings of the IEEE conference on computer vision and pattern recognition* (2014), pp. 2814–2821.
- [ZSL*15] ZHANG J., SCLAROFF S., LIN Z., SHEN X., PRICE B., MECH R.: Minimum barrier salient object detection at 80 fps. In *Proceedings of the IEEE international conference on computer vision* (2015), pp. 1404–1412.
- [ZSQ*17] ZHAO H., SHI J., QI X., WANG X., JIA J.: Pyramid scene parsing network. In *Proceedings of the IEEE conference on computer vision and pattern recognition* (2017), pp. 2881–2890.
- [ZTZ*17] ZHANG R., TANG S., ZHANG Y., LI J., YAN S.: Scale-adaptive convolutions for scene parsing. In *Proceedings of the IEEE International Conference on Computer Vision* (2017), pp. 2031–2039.
- [ZW19] ZHAO T., WU X.: Pyramid feature attention network for saliency detection. In *Proceedings of the IEEE/CVF Conference on Computer Vision and Pattern Recognition* (2019), pp. 3085–3094.
- [ZWL*17] ZHANG P., WANG D., LU H., WANG H., RUAN X.: Amulet: Aggregating multi-level convolutional features for salient object detection. In *Proceedings of the IEEE International Conference on Computer Vision* (2017), Proceedings of the IEEE International Conference on Computer Vision, pp. 202–211.
- [ZWQ*18] ZHANG X., WANG T., QI J., LU H., WANG G.: Progressive attention guided recurrent network for salient object detection. In *Proceedings of the IEEE Conference on Computer Vision and Pattern Recognition* (2018), pp. 714–722.
- [ZXL*20] ZHOU H., XIE X., LAI J.-H., CHEN Z., YANG L.: Interactive two-stream decoder for accurate and fast saliency detection. In *Proceedings of the IEEE/CVF Conference on Computer Vision and Pattern Recognition* (2020), pp. 9141–9150.
- [ZZL*18] ZHAO H., ZHANG Y., LIU S., SHI J., LOY C. C., LIN D., JIA J.: Psanet: Point-wise spatial attention network for scene parsing. In *Proceedings of the European Conference on Computer Vision (ECCV)* (2018), pp. 267–283.